

Witnessing quantum resource conversion within deterministic quantum computation using one pure superconducting qubit

W. Wang,^{1,*} J. Han,^{1,*} B. Yadin,² Y. Ma,¹ J. Ma,¹ W. Cai,¹ Y. Xu,¹ L. Hu,¹ H. Wang,¹ Y. P. Song,¹ Mile Gu,^{3,4,5,†} and L. Sun^{1,‡}

¹Center for Quantum Information, Institute for Interdisciplinary Information Sciences, Tsinghua University, Beijing 100084, China

²Atomic and Laser Physics, Clarendon Laboratory, University of Oxford, Parks Road, Oxford, OX1 3PU, United Kingdom

³School of Physical and Mathematical Sciences, Nanyang Technological University, Singapore 639673, Republic of Singapore

⁴Complexity Institute, Nanyang Technological University, Singapore 639673, Republic of Singapore

⁵Centre for Quantum Technologies, National University of Singapore,

3 Science Drive 2, Singapore 117543, Republic of Singapore

Deterministic quantum computation with one qubit (DQC1) is iconic in highlighting that exponential quantum speedup may be achieved with negligible entanglement. Its discovery catalyzed heated study of general quantum resources, and various conjectures regarding their role in DQC1's performance advantage. Coherence and discord are prominent candidates, respectively characterizing non-classicality within localized and correlated systems. Here we realize DQC1 within a superconducting system, engineered such that the dynamics of coherence and discord can be tracked throughout its execution. We experimentally confirm that DQC1 acts as a resource converter, consuming coherence to generate discord during its operation. Our results highlight superconducting circuits as a promising platform for both realizing DQC1 and related algorithms, and experimentally characterizing resource dynamics within quantum protocols.

Quantum technologies promise to deliver advantages in wide range of information processing tasks from secure communication [1, 2], solving classically intractable problems [3, 4] to the simulation of complex systems [5–7]. The historical view held that entanglement enabled this quantum advantage, a quantum resource that plays pivotal roles in many quantum-enhanced protocols [8]. However, this picture is incomplete. For example, universal quantum computation has been shown to be achievable with little entanglement [9]. The deterministic quantum computation with one qubit (DQC1) model of computation provides another noteworthy counterpoint [10]. The protocol enables potential exponential quantum speedup in evaluating the normalized trace of unitary matrices [11, 12], and its outputs are hard to sample classically [13, 14], yet contains little or no entanglement. This motivated a heated search for alternative explanations regarding its source of quantum advantage [15], and catalyzed the recognition that non-classicality comes in many forms.

Iconic among such developments was discord [16], capturing a more robust form of correlations that can persist in environments where entanglement vanishes. Quantum resources were also proposed to describe non-classical properties to individual systems. This resulted in a framework for quantifying non-classicality within coherent quantum superpositions [17] that has since undergone extensive study [18–33]. Meanwhile, different resources were shown to be convertible into each other, a key example being the use of coherence as a resource for generating quantum correlations [24–26, 34]. The manipulation and interplay of these resources is considered a crucial element for understanding the origin of the power of quantum protocols. Indeed, current propositions of how DQC1 gains its operation power include the build-up of discord [15] and, more recently, the conversion of coherence to quantum correlations [25].

Here we realize the DQC1 algorithm within a superconducting system with a circuit quantum electrodynamics

(QED) architecture [35–37], and monitor the interplay between coherence and discord in the DQC1 model. We implement the algorithm by coherent control and quantum non-demolition (QND) projective measurements on a single pure superconducting qubit dispersively coupled to a harmonic oscillator that can potentially provide a maximally-mixed state with arbitrary dimension. In particular, in our experiment the maximally-mixed state with a dimension of eight is generated with repeated application of Kraus rank-2 channels in an adaptive fashion [38] and we perform full joint state tomography on the combined system to characterize the behavior of coherence and discord in the algorithm. Even in the presence of experimental imperfections, we verify that, as theoretically predicted in Ref. 25, the amount of discord generated during the computation is upper bounded by the consumption of the initial coherence of the system. Our work provides the first experimental characterization of resource conversion dynamics within DQC1, and extends previous experimental realizations of DQC1 in linear optics [39] and liquid-state nuclear magnetic resonance [40] to a new technological medium.

Coherence is taken to mean the superposition of states in some basis set $\{|i\rangle\}$ [17, 41, 42]. In this work, we focus on one measure: the relative entropy of coherence [17],

$$C(\rho) = S(\rho^{diag}) - S(\rho), \quad (1)$$

where $S(\cdot)$ is the von Neumann entropy and ρ^{diag} is the state obtained by removing the off-diagonal elements of ρ in the reference basis $\{|i\rangle\}$.

In a multipartite system, the quantumness of correlations between subsystems A_1, \dots, A_n may be quantified with the global quantum discord $D(\rho_{A_1, \dots, A_n})$ [43]. This is defined as the excess of coherence in the global state ρ_{A_1, \dots, A_n} over the local states $\rho_{A_1}, \dots, \rho_{A_n}$, minimized over all basis choices for each subsystem (see [44] for details).

The DQC1 protocol is illustrated in Fig. 1. The quantum circuit is fed with $n + 1$ qubits, consisting of one pure an-

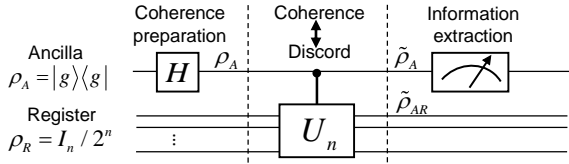


FIG. 1. **DQC1 model.** Initially the ancilla qubit is prepared in a pure ground state and the register qubits are prepared in a maximally-mixed state. Coherence in the quantum system is then prepared in the ancilla qubit by a Hadamard gate and converted into discord by a controlled operation U_n . Measurements of $\langle \sigma_x \rangle$ and $\langle \sigma_y \rangle$ on the ancilla qubit give the real and imaginary parts of $\text{Tr}(U_n)/2^n$ respectively.

cilla qubit and n maximally-mixed register qubits. As noted in Ref. 25, coherence-to-discord conversion takes place in this algorithm. Specifically, coherence is initially generated in the ancilla qubit by a Hadamard gate. Then a controlled- U gate is performed to correlate the ancilla and the register qubits, and thus create discord between the ancilla and register qubits at the cost of the coherence in the ancilla qubit. Note that the control basis of the gate is taken to be the reference basis for which there is no coherence. This process is encapsulated in the following inequality:

$$D(\tilde{\rho}_{AR}) \leq \Delta C(\rho_A), \quad (2)$$

where $\tilde{\rho}_{AR}$ is the joint state of the $n + 1$ qubits after the controlled- U gate, $\Delta C(\rho_A) = C(\rho_A) - C(\tilde{\rho}_A)$ is the coherence consumption during the controlled- U gate, with ρ_A and $\tilde{\rho}_A$ the states of the ancilla qubit before and after the controlled- U gate, respectively.

We realize the DQC1 algorithm using a superconducting transmon qubit dispersively coupled to two waveguide cavity resonators [36, 45–48], as shown in Fig. 2a. The transmon qubit has an energy relaxation time $T_1 = 30 \mu\text{s}$ and a pure dephasing time $T_\phi = 120 \mu\text{s}$. One of the cavities (storage cavity) has a long photon lifetime of $\tau_s = 143 \mu\text{s}$. The Fock states in this storage cavity (composing the register qubits) and the transmon qubit (as the ancilla) constitute the bipartite parts of the DQC1 circuit [16]. The other short-lived cavity with a photon lifetime $\tau_r = 44 \text{ ns}$ is used to readout the ancilla qubit. High fidelity and QND single-shot measurements of the ancilla can be achieved with the help of a phase-sensitive Josephson bifurcation amplifier [49–52]. Each readout measurement throughout our experiment returns a digitized value of the qubit state. The experimental apparatus and readout properties are similar to earlier reports in Refs. 53 and 54.

The ancilla qubit and storage cavity are well described by the dispersive Hamiltonian (omitting small high-order nonlinearities)

$$H/\hbar = \omega_s a^\dagger a + \omega_a |e\rangle\langle e| - \chi a^\dagger a |e\rangle\langle e| \quad (3)$$

where a^\dagger (a) is the creation (annihilation) operator of the storage cavity, $|e\rangle$ is the excited state of the ancilla qubit, and $\chi/2\pi = 1.90 \text{ MHz}$ is the dispersive interaction strength between the qubit and the storage cavity. This strong dispersive

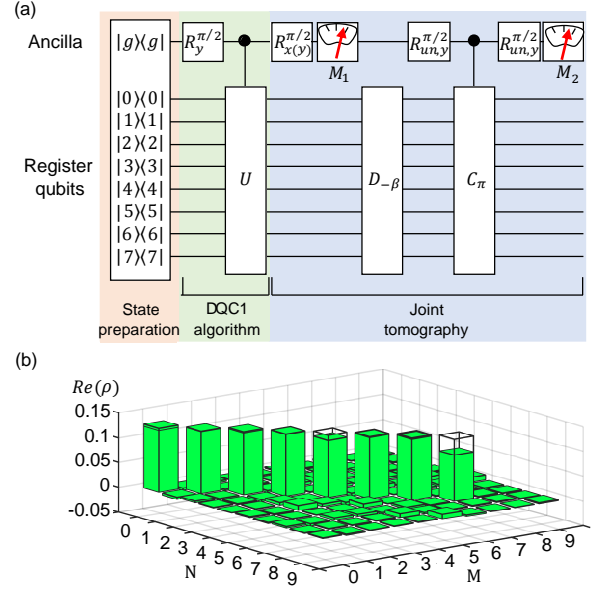


FIG. 2. **Experimental quantum circuit to measure the conversion between coherence and quantum correlations with a DQC1 model.** (a) The whole process can be divided into three parts: state preparation, DQC1 algorithm, and joint tomography measurement. The maximally-mixed state ($\sum_{k=0}^7 |k\rangle\langle k|$) of the initial registers is deterministically generated through a quantum channel construction based on QND measurements of the ancilla and adaptive control of the ancilla-register system. The $R_y^{\pi/2}$ operation to create input coherence in the DQC1 algorithm and the following $R_{x(y)}^{\pi/2}$ operations before M_1 in the joint tomography are all generated by GRAPE to compensate the extra phases corresponding to different register states due to the dispersive interaction during these gates, such that the gate operations are independent of the states of the register qubits. The controlled- U gate is realized through an appropriate ancilla-register interaction time and is used to convert coherence to discord. To characterize the ancilla-register system, joint tomography is performed by correlating the ancilla tomography and subsequent register Wigner tomography. In the joint tomography, the two $\pi/2$ rotations $R_{un,y}^{\pi/2}$ before and after the controlled π phase gate C_π are unconditional gates with a Gaussian envelope of $\sigma = 5 \text{ ns}$. (b) Real part of the reconstructed density matrix (truncated to maximum photon number state $N_{\text{max}} = 9$) of the initial register qubits with a fidelity of 0.977.

coupling gives rise to the ancilla-register entangling operation, allowing for the controlled- U operation in the DQC1 algorithm. The readout cavity has been neglected since it remains in vacuum unless a measurement is performed.

Harmonic oscillators play important roles in quantum information processing [53, 55–58] largely due to their infinite dimension and long coherence times. Here we take advantage of these characteristics to use multiple excitations of a harmonic cavity oscillator as register qubit states. In our experiment, we choose the lowest eight Fock states $\{|0\rangle, |1\rangle, \dots, |7\rangle\}$ in the cavity field whose computational space is equivalent to that of three register qubits, namely $\{|000\rangle, |001\rangle, \dots, |111\rangle\}$ respectively. This gives the DQC1 model in our experiment

with $n = 3$ register qubits.

Our experimental sequence is depicted in Fig. 2a. The whole process can be divided into three parts: state preparation, DQC1 algorithm, and joint tomography measurement. The state preparation starts with a pure ancilla qubit ground state $|g\rangle\langle g|$ by post-selection. The maximally-mixed state as required by the DQC1 model is deterministically generated through a quantum channel construction based on QND measurements of the ancilla and adaptive control of the ancilla-register system [38]. All the adaptive control pulses are numerically calculated with the Gradient Ascent Pulse Engineering (GRAPE) method [59, 60] and the generated maximally-mixed state has a fidelity of 0.977, whose reconstructed density matrix based on the measured Wigner function is shown in Fig. 2b. The state fidelity is defined as $F(\rho_{\text{exp}}, \rho_{\text{ideal}}) = \text{tr} \sqrt{\sqrt{\rho_{\text{ideal}}} \rho_{\text{exp}} \sqrt{\rho_{\text{ideal}}}}$. The protocol for the realization of the maximally-mixed state is shown in [44]. Note that the register qubits do not contribute any coherence to the combined system.

In the following DQC1 algorithm, coherence preparation is performed by an ancilla qubit operation $R_y^{\pi/2}$ corresponding to a $\pi/2$ rotation around the y -axis on the Bloch sphere, having the same action here as a Hadamard gate. Note that this $R_y^{\pi/2}$ operation and the following $R_{x(y)}^{\pi/2}$ operations before M_1 in the joint tomography are also generated by GRAPE to compensate the extra phases during these ‘‘Hadamard’’ gates, such that the gate operations are independent of the states of the register qubits (see [44]). Consequently, the system is prepared in a product state $\rho_{AR} = (|g\rangle + |e\rangle)(\langle g| + \langle e|) \otimes \sum_{k=0}^7 |k\rangle\langle k|$ (ignoring normalization). A conditional cavity phase shift $C_\varphi = |g\rangle\langle g| \otimes \mathbf{1} + |e\rangle\langle e| \otimes e^{i\varphi a^\dagger a}$ is the mechanism of the controlled- U gate, where $\varphi = \chi t$ is acquired from the free evolution of the dispersive Hamiltonian Eq. 3 for a time interval t . As a result, the controlled- U gate can be described as $|g\rangle\langle g| \otimes \mathbf{1} + |e\rangle\langle e| \otimes U$, where

$$U = \begin{pmatrix} 1 & 0 & \dots & 0 \\ 0 & e^{i\varphi} & \dots & 0 \\ \vdots & \vdots & \ddots & \vdots \\ 0 & 0 & \dots & e^{i7\varphi} \end{pmatrix} \quad (4)$$

in the computational Hilbert space. Note that in the Fock state basis, the controlled- U is an incoherent operation. After the controlled- U gate, the system evolves to $\tilde{\rho}_{AR}$.

To observe the bipartite system, we finally perform a joint measurement of the coupled ancilla-register system with two sequential QND measurements of the ancilla qubit and the register qubits, following a technique similar to that previously demonstrated in Ref. 61. As shown in Fig. 2b, the ancilla qubit detections along one of the three basis vectors X, Y , and Z are first performed with or without an appropriate pre-rotation $R_{x(y)}^{\pi/2}$ followed by a z -basis measurement M_1 . These measurements alone can give a full tomography of the ancilla. Then a Wigner tomography of the register qubit is performed by measuring the cavity observable $P(\beta)$ which is

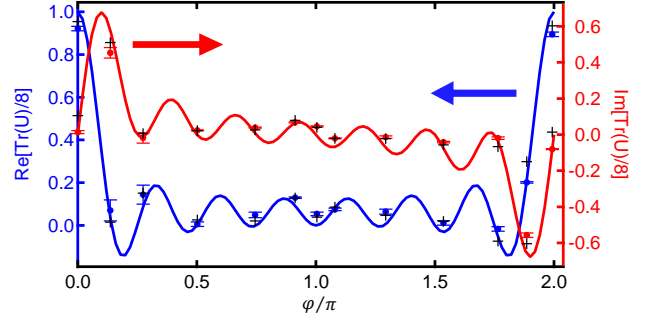


FIG. 3. **DQC1 algorithm output.** The real and imaginary parts of the normalized trace $\text{Tr}(U)/8$ are measured for different φ . All data (points) are averaged with over 10^7 measurements and error bars correspond to one standard deviation. The solid lines show theoretical expectations. Crosses present the simulated results including all decoherence channels. Experiment results agree well with both theory and simulation even with the presence of decoherence processes from both ancilla and register qubits.

a combination of the cavity’s displacement operation $D_{-\beta}$ and a parity measurement P of the cavity. The parity measurement is realized in a Ramsey-type experiment of the ancilla qubit, where a conditional cavity π phase shift C_π is sandwiched in between two unconditional qubit rotations $R_{un,y}^{\pi/2}$ (a Gaussian envelope with $\sigma = 5$ ns) followed by another z -basis measurement M_2 [46, 47, 62, 63]. After the qubit tomography measurement M_1 , the qubit is at a specific known state and the correlation of M_1 and M_2 determines the parity of the register. Multiplication of the ancilla qubit detection σ_i (in the qubit Pauli set $\{I, X, Y, Z\}$) and the register Wigner tomography $W(\beta) = \frac{2}{\pi} \langle P(\beta) \rangle$ shot-by-shot gives the joint Wigner function [61], defined as:

$$W_i(\beta) = \frac{2}{\pi} \langle \sigma_i P(\beta) \rangle \quad (5)$$

The joint Wigner functions are a complete representation of the combined ancilla-register quantum system. From these functions we reconstruct the combined ancilla-register density matrix $\tilde{\rho}_{AR}$ in a 16-dimensional Hilbert space by a least squares regression using maximum likelihood estimation with the only constraints that the reconstructed density matrix is positive semi-definite with trace equal to one [61, 64]. Based on the obtained density matrix $\tilde{\rho}_{AR}$, we can derive the remaining coherence $C(\tilde{\rho}_A)$ and the created discord $D(\tilde{\rho}_{AR})$ [44], where $\tilde{\rho}_A$ is the partial trace of $\tilde{\rho}_{AR}$ over the registers.

The initial coherence is generated by the ancilla qubit operation $R_y^{\pi/2}$ and is first characterized to be $C(\rho_A) = 0.894$ by a qubit tomography immediately after this coherent operation, while the ancilla qubit state fidelity is 0.993 (see [44]). The reduction is mainly due to a qubit decay process during the tomography measurement and the imperfection of $R_y^{\pi/2}$ in the presence of the maximally-mixed state. This initial coherence built in the ancilla state is then to be consumed in order to correlate the ancilla and the register qubits, and thus is used as a reference for the coherence consumption. We next

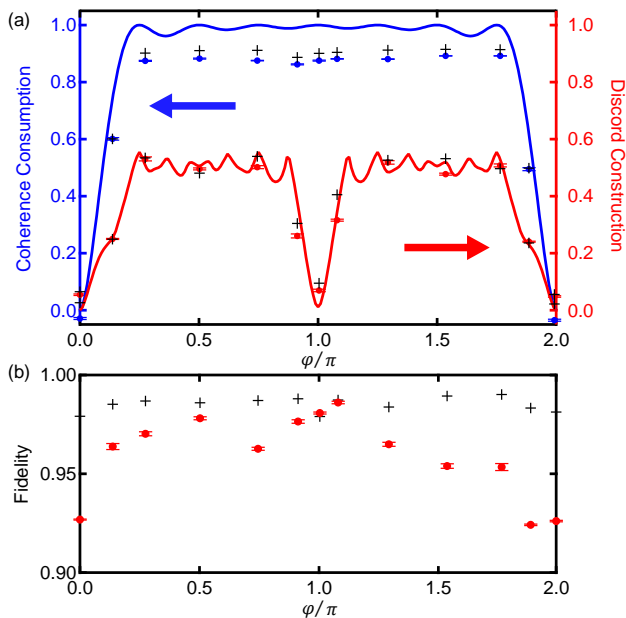


FIG. 4. **The coherence consumption $\Delta C(\rho_A)$ and discord production $D(\tilde{\rho}_{AR})$ as a function of phase φ in the DQC1 model.** (a) Theoretical expectations are shown with solid lines. Dots give the experimental results. In the experiment, each point in the joint Wigner functions has been averaged over 3000 single-shot joint ancilla and register measurements, and the standard deviation in $\Delta C(\rho_A)$ and $D(\tilde{\rho}_{AR})$ are estimated by bootstrapping on the measured joint Wigner functions [61]. Crosses present the simulated data including all decoherence channels with both the ancilla and register qubits. The measured $\Delta C(\rho_A)$ agrees fairly well with the theoretical one with a small gap at the middle plateau. This gap comes from the imperfect generation and measurement of the initial coherence $C(\rho_A) = 0.894$ while the ancilla state fidelity is 0.993 to the ideal state $(|g\rangle + |e\rangle)/\sqrt{2}$ after the $R_y^{\pi/2}$ operation. The measured $D(\tilde{\rho}_{AR})$, in excellent agreement with the theoretical expectation, captures all the important features as in the theoretical curve and is unambiguously lower than $\Delta C(\rho_A)$ as expected. (b) The fidelity of the measured $\tilde{\rho}_{AR}$ compared to the ideal ones with an average of 0.96.

show the results after applying the controlled- U gate in the DQC1 model. The normalized trace of U is encoded in the ancilla qubit and can be recovered from the result of M_1 , as shown in Fig. 3. Although there are decoherence processes with both ancilla and register qubits, the experimental results (dots) agree well with the exact theoretical expectation (lines) and the numerical simulation (crosses) that involves all imperfection channels, suggesting the robustness of the protocol.

We finally show in Fig. 4 the coherence consumption $\Delta C(\rho_A)$ and discord production $D(\tilde{\rho}_{AR})$ in the DQC1 model as a function of phase φ in the controlled- U gate which varies over the range $0 \leq \varphi \leq 2\pi$. Theoretical expectations of $\Delta C(\rho_A)$ and $D(\tilde{\rho}_{AR})$ for an ideal system without any decoherence are shown as solid lines for comparison. Both curves are symmetric around $\varphi = \pi$. At $\varphi = \pi$, the controlled- U gate is expected to transform the qubit-register system into a classically correlated state without any discord. At $\varphi = \pi/2, \pi, 3\pi/2$, after tracing out the register state the an-

ancilla qubit is in a maximally-mixed state. In these cases, the original coherence is completely consumed by the controlled- U operation. The gap between the expected solid lines means that, even theoretically, coherence can not be fully converted to discord. The non-monotonic oscillations in the theoretical curves are not fully understood yet and need further investigation.

The experimental results for both $\Delta C(\rho_A)$ and $D(\tilde{\rho}_{AR})$ are depicted as dots and are indeed quite symmetric around $\varphi = \pi$, and capture all the important features in the theoretical curves. The measured coherence consumption agrees fairly well with theory. The small gap at the middle plateau comes from the imperfect generation and measurement of the initial coherence $C(\rho_A) = 0.894$. The measured produced discord agrees extremely well with the theoretical expectation. All measured $D(\tilde{\rho}_{AR})$ are indeed significantly lower than the measured $\Delta C(\rho_A)$, successfully demonstrating Eq. 2. Figure 4b shows the state fidelity of the ancilla-register system at each φ based on the measured $\tilde{\rho}_{AR}$. All fidelities are above 0.92, demonstrating the good control of our system throughout the process.

We note that in Eq. 3 the higher order corrections to the dispersive term, such as $(\chi'/2)a^\dagger a^\dagger aa|e\rangle\langle e|$ (χ' is typically more than two orders of magnitude smaller than χ), have been ignored because of their small contribution to φ compared to the dispersive term in the small photon number limit. However, these higher order non-linear terms in principle allow for generating arbitrary controlled- U by repeated applications of appropriate cavity displacements followed by appropriate waiting, provided the system has enough coherence [65–68].

In summary, we have experimentally demonstrated and quantified quantum resource conversion in the DQC1 model. We show that coherence is converted into the quantum discord that is considered as the resource in DQC1 [15]. The produced discord is unambiguously demonstrated to be lower than the coherence consumption. This experiment reveals the potential of superconducting circuits as a versatile platform for investigating and even deepening our understanding of resource dynamics in quantum information.

A natural extension of the present work is to chain multiple DQC1 circuits together. Provided the register qubits are not reset between iterations, the resulting circuit enables a variant of Shor’s algorithm [69, 70]. Here, each iteration converts an additional bit of coherence into quantum correlations, enabling study of resource conversion dynamics within the iconic quantum factoring protocol. Our architecture is also suitable for the “power of one pure qumode” protocol – in which the control qubit in DQC1 is replaced with a continuous variable mode to form a hybrid model of computation that combines discrete and continuous variables [71]. Its realization could enable hybrid factoring algorithms, and aid the study of how continuous and discrete notions of non-classicality interact. Each of these developments would provide a promising experimental platform for studying quantum resource dynamics within more complex settings.

* These two authors contributed equally to this work.

† mgu@quantumcomplexity.org

‡ luyansun@tsinghua.edu.cn

- [1] N. Gisin, G. Ribordy, W. Tittel, and H. Zbinden, “Quantum cryptography,” *Rev. Mod. Phys.* **74**, 145 (2002).
- [2] V. Scarani, H. Bechmann-Pasquinucci, N. J. Cerf, M. Dušek, N. Lütkenhaus, and M. Peev, “The security of practical quantum key distribution,” *Rev. Mod. Phys.* **81**, 1301 (2009).
- [3] P. W. Shor, “Algorithms for quantum computation: Discrete logarithms and factoring,” in *Foundations of Computer Science, 1994 Proceedings., 35th Annual Symposium on* (IEEE, 1994) pp. 124–134.
- [4] L. K. Grover, “A fast quantum mechanical algorithm for database search,” in *Proceedings of the twenty-eighth annual ACM symposium on Theory of computing* (ACM, 1996) pp. 212–219.
- [5] S. Lloyd, “Universal quantum simulators,” *Science* **273**, 1073 (1996).
- [6] I. M. Georgescu, S. Ashhab, and F. Nori, “Quantum simulation,” *Rev. Mod. Phys.* **86**, 153 (2014).
- [7] M. Gu, K. Wiesner, E. Rieper, and V. Vedral, “Quantum mechanics can reduce the complexity of classical models,” *Nat. Commun.* **3**:762 (2012).
- [8] R. Horodecki, P. Horodecki, M. Horodecki, and K. Horodecki, “Quantum entanglement,” *Rev. Mod. Phys.* **81**, 865 (2009).
- [9] M. Van den Nest, “Universal quantum computation with little entanglement,” *Phys. Rev. Lett.* **110**, 060504 (2013).
- [10] E. Knill and R. Laflamme, “Power of one bit of quantum information,” *Phys. Rev. Lett.* **81**, 5672 (1998).
- [11] A. Datta and G. Vidal, “Role of entanglement and correlations in mixed-state quantum computation,” *Phys. Rev. A* **75**, 042310 (2007).
- [12] M. Hor-Meyll, D. S. Tasca, S. P. Walborn, P. H. S. Ribeiro, M. M. Santos, and E. I. Duzzioni, “Deterministic quantum computation with one photonic qubit,” *Phys. Rev. A* **92**, 012337 (2015).
- [13] T. Morimae, K. Fujii, and J. F. Fitzsimons, “Hardness of classically simulating the one-clean-qubit model,” *Phys. Rev. Lett.* **112**, 130502 (2014).
- [14] K. Fujii, H. Kobayashi, T. Morimae, H. Nishimura, S. Tamate, and S. Tani, “Impossibility of classically simulating one-clean-qubit model with multiplicative error,” *Phys. Rev. Lett.* **120**, 200502 (2018).
- [15] A. Datta, A. Shaji, and C. M. Caves, “Quantum discord and the power of one qubit,” *Phys. Rev. Lett.* **100**, 050502 (2008).
- [16] K. Modi, A. Brodutch, H. Cable, T. Paterek, and V. Vedral, “The classical-quantum boundary for correlations: Discord and related measures,” *Rev. Mod. Phys.* **84**, 1655 (2012).
- [17] T. Baumgratz, M. Cramer, and M. B. Plenio, “Quantifying coherence,” *Phys. Rev. Lett.* **113**, 140401 (2014).
- [18] D. Girolami, “Observable measure of quantum coherence in finite dimensional systems,” *Phys. Rev. Lett.* **113**, 170401 (2014).
- [19] T. R. Bromley, M. Cianciaruso, and G. Adesso, “Frozen quantum coherence,” *Phys. Rev. Lett.* **114**, 210401 (2015).
- [20] X. Yuan, H. Zhou, Z. Cao, and X. Ma, “Intrinsic randomness as a measure of quantum coherence,” *Phys. Rev. A* **92**, 022124 (2015).
- [21] S. Cheng and M. J. W. Hall, “Complementarity relations for quantum coherence,” *Phys. Rev. A* **92**, 042101 (2015).
- [22] Y. Yao, X. Xiao, L. Ge, and C. P. Sun, “Quantum coherence in multipartite systems,” *Phys. Rev. A* **92**, 022112 (2015).
- [23] L.-H. Shao, Z. Xi, H. Fan, and Y. Li, “Fidelity and trace-norm distances for quantifying coherence,” *Phys. Rev. A* **91**, 042120 (2015).
- [24] A. Streltsov, U. Singh, H. S. Dhar, M. N. Bera, and G. Adesso, “Measuring quantum coherence with entanglement,” *Phys. Rev. Lett.* **115**, 020403 (2015).
- [25] J. Ma, B. Yadin, D. Girolami, V. Vedral, and M. Gu, “Converting coherence to quantum correlations,” *Phys. Rev. Lett.* **116**, 160407 (2016).
- [26] E. Chitambar, A. Streltsov, S. Rana, M. N. Bera, G. Adesso, and M. Lewenstein, “Assisted distillation of quantum coherence,” *Phys. Rev. Lett.* **116**, 070402 (2016).
- [27] A. Winter and D. Yang, “Operational resource theory of coherence,” *Phys. Rev. Lett.* **116**, 120404 (2016).
- [28] C. Napoli, T. R. Bromley, M. Cianciaruso, M. Piani, N. Johnston, and G. Adesso, “Robustness of coherence: An operational and observable measure of quantum coherence,” *Phys. Rev. Lett.* **116**, 150502 (2016).
- [29] B. Yadin, J. Ma, D. Girolami, M. Gu, and V. Vedral, “Quantum processes which do not use coherence,” *Phys. Rev. X* **6**, 041028 (2016).
- [30] S. Rana, P. Parashar, and M. Lewenstein, “Trace-distance measure of coherence,” *Phys. Rev. A* **93**, 012110 (2016).
- [31] X. Yuan, K. Liu, Y. Xu, W. Wang, Y. Ma, F. Zhang, Z. Yan, R. Vijay, L. Sun, and X. Ma, “Experimental quantum randomness processing using superconducting qubits,” *Phys. Rev. Lett.* **117**, 010502 (2016).
- [32] C. Radhakrishnan, M. Parthasarathy, S. Jambulingam, and T. Byrnes, “Distribution of quantum coherence in multipartite systems,” *Phys. Rev. Lett.* **116**, 150504 (2016).
- [33] J. P. Santos, L. Celeri, G. T. Landi, and M. Paternostro, “The role of quantum coherence in non-equilibrium entropy production,” *npj Quantum Inf.* **5** (2017).
- [34] K. Wu, Z. Hou, Y. Zhao, G. Xiang, C. Li, G. Guo, J. Ma, Q. He, J. Thompson, and M. Gu, “Experimental cyclic inter-conversion between coherence and quantum correlations,” [arXiv:1710.01738](https://arxiv.org/abs/1710.01738) (2017).
- [35] A. Wallraff, D. I. Schuster, A. Blais, L. Frunzio, R.-S. Huang, J. Majer, S. Kumar, S. M. Girvin, and R. J. Schoelkopf, “Circuit quantum electrodynamics: Coherent coupling of a single photon to a cooper pair box,” *Nature* **431**, 162 (2004).
- [36] H. Paik, D. I. Schuster, L. S. Bishop, G. Kirchmair, G. Catelani, A. P. Sears, B. R. Johnson, M. J. Reagor, L. Frunzio, L. I. Glazman, S. M. Girvin, M. H. Devoret, and R. J. Schoelkopf, “Observation of high coherence in josephson junction qubits measured in a three-dimensional circuit qed architecture,” *Phys. Rev. Lett.* **107**, 240501 (2011).
- [37] M. H. Devoret and R. J. Schoelkopf, “Superconducting circuits for quantum information: An outlook,” *Science* **339**, 1169 (2013).
- [38] C. Shen, K. Noh, V. V. Albert, S. Krastanov, M. H. Devoret, R. J. Schoelkopf, S. M. Girvin, and L. Jiang, “Quantum channel construction with circuit quantum electrodynamics,” *Phys. Rev. B* **95**, 134501 (2017).
- [39] B. P. Lanyon, M. Barbieri, M. P. Almeida, and A. G. White, “Experimental quantum computing without entanglement,” *Phys. Rev. Lett.* **101**, 200501 (2008).
- [40] G. Passante, O. Moussa, D. A. Trottier, and R. Laflamme, “Experimental detection of nonclassical correlations in mixed-state quantum computation,” *Phys. Rev. A* **84**, 044302 (2011).
- [41] A. Streltsov, G. Adesso, and M. B. Plenio, “Colloquium : Quantum coherence as a resource,” *Rev. Mod. Phys.* **89**, 041003 (2017).
- [42] The reference basis $\{|i\rangle\}$ typically corresponds to be a basis that

- is considered classical for physical reasons. Examples include the energy eigenbasis, or the basis a system naturally decoheres to when left in contact with the environment.
- [43] C. C. Rulli and M. S. Sarandy, “Global quantum discord in multipartite systems,” *Phys. Rev. A* **84**, 042109 (2011).
- [44] Supplementary Materials.
- [45] G. Kirchmair, B. Vlastakis, Z. Leghtas, S. E. Nigg, H. Paik, E. Ginossar, M. Mirrahimi, L. Frunzio, S. M. Girvin, and R. J. Schoelkopf, “Observation of quantum state collapse and revival due to the single-photon Kerr effect,” *Nature* **495**, 205 (2013).
- [46] B. Vlastakis, G. Kirchmair, Z. Leghtas, S. E. Nigg, L. Frunzio, S. M. Girvin, M. Mirrahimi, M. H. Devoret, and R. J. Schoelkopf, “Deterministically encoding quantum information using 100-photon Schrödinger cat states,” *Science* **342**, 607 (2013).
- [47] L. Sun, A. Petrenko, Z. Leghtas, B. Vlastakis, G. Kirchmair, K. M. Sliwa, A. Narla, M. Hatridge, S. Shankar, J. Blumoff, L. Frunzio, M. Mirrahimi, M. H. Devoret, and R. J. Schoelkopf, “Tracking photon jumps with repeated quantum non-demolition parity measurements,” *Nature* **511**, 444 (2014).
- [48] K. Liu, Y. Xu, W. Wang, S.-B. Zheng, T. Roy, S. Kundu, M. Chand, A. Ranadive, R. Vijay, Y. Song, *et al.*, “A twofold quantum delayed-choice experiment in a superconducting circuit,” *Science Advances* **3**, e1603159 (2017).
- [49] M. Hatridge, R. Vijay, D. H. Slichter, J. Clarke, and I. Siddiqi, “Dispersive magnetometry with a quantum limited SQUID parametric amplifier,” *Phys. Rev. B* **83**, 134501 (2011).
- [50] T. Roy, S. Kundu, M. Chand, A. M. Vadiraj, A. Ranadive, N. Nehra, M. P. Patankar, J. Aumentado, A. A. Clerk, and R. Vijay, “Broadband parametric amplification with impedance engineering: Beyond the gain-bandwidth product,” *Appl. Phys. Lett.* **107**, 262601 (2015).
- [51] A. Kamal, A. Marblestone, and M. H. Devoret, “Signal-to-pump back action and self-oscillation in double-pump Josephson parametric amplifier,” *Phys. Rev. B* **79**, 184301 (2009).
- [52] K. W. Murch, S. J. Weber, C. Macklin, and I. Siddiqi, “Observing single quantum trajectories of a superconducting quantum bit,” *Nature* **502**, 211 (2013).
- [53] L. Hu, Y. Ma, W. Cai, X. Mu, Y. Xu, W. Wang, Y. Wu, H. Wang, Y. Song, C. Zou, S. M. Girvin, L.-M. Duan, and L. Sun, “Quantum error correction and universal gate set on a binomial bosonic logical qubit,” *Nat. Phys.* **15**, 503 (2019).
- [54] L. Hu, X. Mu, W. Cai, Y. Ma, Y. Xu, H. Wang, Y. Song, C.-L. Zou, and L. Sun, “Experimental repetitive quantum channel simulation,” *Sci. Bull.* **63**, 1551 (2018).
- [55] V. Bužek and P. L. Knight, “Quantum interference, superposition states of light, and nonclassical effects,” *Progress in Optics* **34**, 1 (1995).
- [56] Z. Leghtas, G. Kirchmair, B. Vlastakis, R. J. Schoelkopf, M. H. Devoret, and M. Mirrahimi, “Hardware-efficient autonomous quantum memory protection,” *Phys. Rev. Lett.* **111**, 120501 (2013).
- [57] N. Ofek, A. Petrenko, R. Heeres, P. Reinhold, Z. Leghtas, B. Vlastakis, Y. Liu, L. Frunzio, S. M. Girvin, L. Jiang, M. Mirrahimi, M. H. Devoret, and R. J. Schoelkopf, “Extending the lifetime of a quantum bit with error correction in superconducting circuits,” *Nature* **536**, 441 (2016).
- [58] M. H. Michael, M. Silveri, R. T. Brierley, V. V. Albert, J. Salmilehto, L. Jiang, and S. M. Girvin, “New class of quantum error-correcting codes for a bosonic mode,” *Phys. Rev. X* **6**, 031006 (2016).
- [59] N. Khaneja, T. Reiss, C. Kehlet, T. Schulte-Herbrüggen, and S. J. Glaser, “Optimal control of coupled spin dynamics: design of NMR pulse sequences by gradient ascent algorithms,” *J. Magn. Reson.* **172**, 296 (2005).
- [60] P. de Fouquieres, S. Schirmer, S. Glaser, and I. Kuprov, “Second order gradient ascent pulse engineering,” *J. Magn. Reson.* **212**, 412 (2011).
- [61] B. Vlastakis, A. Petrenko, N. Ofek, L. Sun, Z. Leghtas, K. Sliwa, Y. Liu, M. Hatridge, J. Blumoff, L. Frunzio, M. Mirrahimi, L. Jiang, M. H. Devoret, and R. J. Schoelkopf, “Characterizing entanglement of an artificial atom and a cavity cat state with Bell’s inequality,” *Nat. Commun.* **6**:8970 (2015).
- [62] L. G. Lutterbach and L. Davidovich, “Method for direct measurement of the wigner function in cavity qed and ion traps,” *Phys. Rev. Lett.* **78**, 2547 (1997).
- [63] P. Bertet, A. Auffeves, P. Maioli, S. Osnaghi, T. Meunier, M. Brune, J. M. Raimond, and S. Haroche, “Direct measurement of the wigner function of a one-photon fock state in a cavity,” *Phys. Rev. Lett.* **89**, 200402 (2002).
- [64] J. A. Smolin, J. M. Gambetta, and G. Smith, “Efficient method for computing the maximum-likelihood quantum state from measurements with additive gaussian noise,” *Phys. Rev. Lett.* **108**, 070502 (2012).
- [65] D. Deutsch, A. Barenco, and A. Ekert, “Universality in quantum computation,” *Proc. R. Soc. London, Ser. A* **449**, 669 (1995).
- [66] S. Lloyd, “Almost any quantum logic gate is universal,” *Phys. Rev. Lett.* **75**, 346 (1995).
- [67] S. L. Braunstein and P. van Loock, “Quantum information with continuous variables,” *Rev. Mod. Phys.* **77**, 513 (2005).
- [68] C.-L. Zou, L. Jiang, X.-B. Zou, and G.-C. Guo, “Filtration and extraction of quantum states from classical inputs,” *Phys. Rev. A* **94**, 013841 (2016).
- [69] S. Parker and M. B. Plenio, “Efficient factorization with a single pure qubit and $\log N$ mixed qubits,” *Phys. Rev. Lett.* **85**, 3049 (2000).
- [70] E. Martín-López, A. Laing, T. Lawson, R. Alvarez, X.-Q. Zhou, and J. L. O’Brien, “Experimental realization of shor’s quantum factoring algorithm using qubit recycling,” *Nat. Photonics* **6**, 773 (2012).
- [71] N. Liu, J. Thompson, C. Weedbrook, S. Lloyd, V. Vedral, M. Gu, and K. Modi, “Power of one qumode for quantum computation,” *Phys. Rev. A* **93**, 052304 (2016).

Supplementary Materials for “Witnessing quantum resource conversion within deterministic quantum computation using one pure superconducting qubit”

W. Wang,^{1,*} J. Han,^{1,*} B. Yadin,² Y. Ma,¹ J. Ma,¹ W. Cai,¹ Y. Xu,¹ L. Hu,¹ H. Wang,¹ Y. P. Song,¹ Mile Gu,^{3,4,5,†} and L. Sun^{1,‡}

¹Center for Quantum Information, Institute for Interdisciplinary Information Sciences, Tsinghua University, Beijing 100084, China

²Atomic and Laser Physics, Clarendon Laboratory, University of Oxford, Parks Road, Oxford, OX1 3PU, United Kingdom

³School of Physical and Mathematical Sciences, Nanyang Technological University, Singapore 639673, Republic of Singapore

⁴Complexity Institute, Nanyang Technological University, Singapore 639673, Republic of Singapore

⁵Centre for Quantum Technologies, National University of Singapore,

3 Science Drive 2, Singapore 117543, Republic of Singapore

I. THEORETICAL PRELIMINARIES

Here we present theoretical preliminaries for calculations of coherence consumption and discord production. Coherence is taken here to mean the superposition of states in some preferred basis set $\{|i\rangle\}$. There is often a natural physical basis to consider – here, it will be the energy basis of the superconducting qubit. The resource theory of coherence [1] provides criteria for determining valid measures of coherence. One first defines the set of states with no coherence \mathcal{I} , or incoherent states, to be all states of the form $\sigma = \sum_i p_i |i\rangle\langle i|$. A good coherence measure must vanish exactly on this set. Next, one defines incoherent operations to be those quantum operations having a set of Kraus operators $\{K_i\}$ with the property $K_i \mathcal{I} K_i^\dagger \in \mathcal{I}$. This condition says that an incoherent operation is never able to create coherence from an incoherent state. The next criterion for a valid coherence measure is then that it cannot increase under an incoherent operation. A number of interesting measures satisfying these criteria have been found [2]. We use the relative entropy of coherence [1], defined as

$$C(\rho) := \min_{\sigma \in \mathcal{I}} S(\rho || \sigma) \quad (S1)$$

$$= S(\rho^{diag}) - S(\rho), \quad (S2)$$

where $S(\rho) = -\text{Tr} \rho \log \rho$ is the von Neumann entropy, $S(\rho || \sigma) = -S(\rho) - \text{Tr} \rho \log \sigma$ is the relative entropy, and ρ^{diag} is the state obtained by removing the off-diagonal elements of ρ in the reference basis $\{|i\rangle\}$.

Quantum discord has a number of characterizations, the first historically being the gap between the total correlations and the classical correlations accessible from local measurements [3, 4]. In a system partitioned into n subsystems $\{A_1, A_2, \dots, A_n\}$, states with vanishing discord are called classically correlated. They take the form $\sum_{k_1, \dots, k_n} p_{k_1, \dots, k_n} |k_1, \dots, k_n\rangle\langle k_1, \dots, k_n|$, where $\{p_{k_1, \dots, k_n}\} \geq 0$, $\sum_{k_1, \dots, k_n} p_{k_1, \dots, k_n} = 1$ and $\{|k_1, \dots, k_n\rangle\} = |k_1\rangle \otimes \dots \otimes |k_n\rangle$ is an arbitrary product basis. Classically correlated states are separable (not entangled), but not every separable state is classically correlated. There are many proposed measures of discord [5, 6]; we focus on one

measure which treats all subsystems equally, named global discord [7]. This is defined by

$$D(\rho_{A_1, \dots, A_n}) = \min_{\Phi^i} S(\rho_{A_1, \dots, A_n} || \Phi^i(\rho_{A_1, \dots, A_n})) - \sum_k S(\rho_{A_k} || \Phi_{A_k}^i(\rho_{A_k})) \quad (S3)$$

where $\Phi^i = \otimes_{j=1}^n \Phi_{A_j}^i$, $\Phi_{A_k}^i(\rho_{A_k}) = \sum_i |i_k\rangle\langle i_k| \rho_{A_k} |i_k\rangle\langle i_k|$ is the dephasing operation, and the minimization is over all dephasing basis choices.

II. REALIZATION OF THE MAXIMALLY-MIXED STATE OF THE REGISTER QUBITS

As pointed out by Lloyd and Viola [8], universal dynamical control of a quantum system can be achieved if one can perform quantum non-demolition (QND) measurements of the system and feedback the measurement results via coherent control. Shen et al. [9] further prove that quantum channel simulation of arbitrary dimension can be efficiently realized with a single ancilla qubit and adaptive control in a binary-tree configuration [10].

Here, we adopt such a method by repeatedly applying Kraus rank-2 channels with real-time feedback control to generate the maximally-mixed state $\sum_{k=0}^7 |k\rangle\langle k|$. Figure S1 shows the three-layer binary tree representation and the experimental sequence of this protocol. All the adaptive control operations are achieved through numerical optimization with the Gradient Ascent Pulse Engineering (GRAPE) method [11, 12], an optimization algorithm designed to numerically find pulses that most accurately realize a unitary operation. The created maximally-mixed state is characterized by the typical Wigner tomography and the reconstructed density matrix is shown in Fig. 2b of the main text with a high state fidelity of 0.977.

III. MANIPULATION OF THE ANCILLARY QUBIT INDEPENDENT OF THE REGISTER STATE AND CALIBRATION OF THE INPUT COHERENCE

In the DQC1 algorithm, initially the ancilla qubit is prepared in a pure ground state and the register qubits are prepared in a maximally-mixed state. Coherence in the quantum system is prepared in the ancilla qubit by a Hadamard gate and

* These two authors contributed equally to this work.

† mgu@quantumcomplexity.org

‡ luyansun@tsinghua.edu.cn

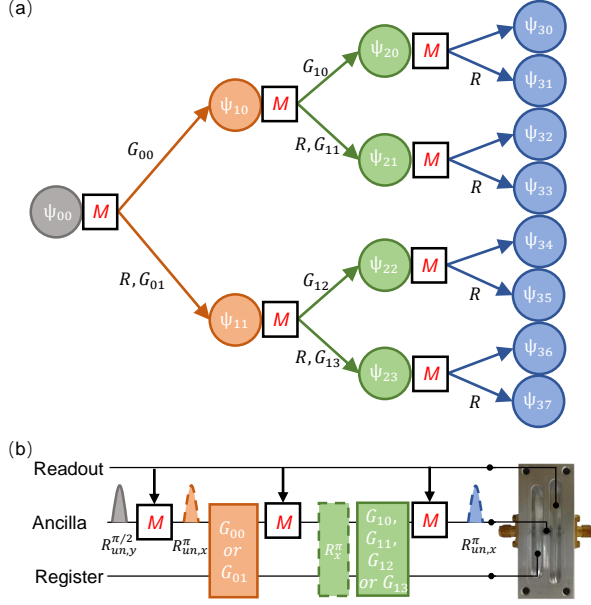


FIG. S1. **Preparation of the initial registers in the maximally-mixed state.** (a) Binary tree representation with a depth $L = 3$. M represents the QND measurement of the ancilla qubit. States $|\psi\rangle$ and adaptive controls G are presented in Table I. All the adaptive control G 's are achieved through numerical optimization with the GRAPE method. R represents a reset process of the ancilla qubit. By implementing three layers of the adaptive operations, we can obtain the maximally-mixed state $\sum_{k=0}^7 |k\rangle\langle k|$. (b) The experimental sequence for preparing the initial register state and optical image of the device with a transmon qubit, as the ancilla qubit, dispersively coupled to two three-dimensional cavities. We first prepare the ancilla-register system in $|\psi_{00}\rangle = (|g\rangle + |e\rangle)/\sqrt{2} \otimes |0\rangle$ from $|g\rangle \otimes |0\rangle$ through an unconditional qubit rotation $R_{un,y}^{\pi/2}$ (a Gaussian envelope with $\sigma = 5$ ns). We then repeatedly measure the ancilla qubit (three layers) along the z -axis. Based on the measurement results, proper unitary operations G_{ij} are applied to change the system state to $|\psi_{i+1,j}\rangle$. If the ancilla is measured in the excited state $|e\rangle$, a reset process “ R ” first flips the qubit to the ground state $|g\rangle$ before the G gate. The reset gates after the first and the third measurements are unconditional π pulses $R_{un,x}^{\pi}$. The one after the second measurement is a numerically optimized pulse R_x^{π} with the GRAPE method, independent of the register state.

then converted into discord by the following controlled operation. To have this algorithm work properly, it is critical that the Hadamard gate on the ancilla qubit is independent of the register state. As the registers are in the maximally-mixed state, photon numbers in the storage cavity are variable. Therefore, a conventional rotation pulse (with a Gaussian envelope) on the ancilla qubit will no longer work because different photon numbers induce different phases on the ancilla qubit – as the duration required to execute the pulse is non-negligible in the context of the coupling strength between the ancilla and the cavity mode. To mitigate these phase errors, we instead use the GRAPE method to realize the Hadamard gate, which does not depend on the number of photons in the cavity mode. The following ancilla rotations (the operations before M_1 in the joint tomography process, Fig. 2a of the main text) also

need to be insensitive to the register state and are realized in the same way.

Figure S2a shows the experimental circuit to calibrate the input coherence, which also confirms the insensitivity of the ancilla qubit rotations to the photon numbers in the storage cavity. The experimental results for the generated $(|g\rangle + |e\rangle)/\sqrt{2}$ when the registers are in the maximally-mixed state are shown in Fig. S2b with a state fidelity of 0.993. The corresponding density matrix contributes 0.894 of the relative entropy of coherence based on Eq. 1 of the main text.

IV. CALIBRATION AND COMPENSATION OF THE MEASUREMENT-INDUCED PHASES

Due to the coupling between the readout cavity and the storage cavity, each measurement induces a phase to the register state. To calibrate this measurement-induced phase, we prepare the registers in $(|0\rangle + |1\rangle)/\sqrt{2}$, $(|0\rangle + |2\rangle)/\sqrt{2}$, ..., $(|0\rangle + |7\rangle)/\sqrt{2}$ respectively, implement the measurement operations repeatedly, and finally measure the probabilities $p(0 + N)$ of the registers along the corresponding basis of $(|0\rangle + |1\rangle)/\sqrt{2}$, $(|0\rangle + |2\rangle)/\sqrt{2}$, ..., $(|0\rangle + |7\rangle)/\sqrt{2}$ (Ramsey-type experiments). The experimental results are shown in Fig. S3. Fitting the curves with damped sinusoidal functions

TABLE I. The states $|\psi\rangle$ and the adaptive control pulses G in the binary-tree realization of the maximally-mixed state. All G 's are achieved through the GRAPE method. The states are not normalized for simplicity.

ψ_{00}	$(g\rangle + e\rangle) \otimes 0\rangle$
ψ_{10}	$ g\rangle \otimes (0\rangle + 7\rangle) + e\rangle \otimes (2\rangle + 5\rangle)$
ψ_{11}	$ g\rangle \otimes (1\rangle + 6\rangle) + e\rangle \otimes (3\rangle + 4\rangle)$
ψ_{20}	$ g\rangle \otimes 7\rangle + e\rangle \otimes 0\rangle$
ψ_{21}	$ g\rangle \otimes 5\rangle + e\rangle \otimes 2\rangle$
ψ_{22}	$ g\rangle \otimes 6\rangle + e\rangle \otimes 1\rangle$
ψ_{23}	$ g\rangle \otimes 4\rangle + e\rangle \otimes 3\rangle$
ψ_{30}	$ g\rangle \otimes 7\rangle$
ψ_{31}	$ g\rangle \otimes 0\rangle$
ψ_{32}	$ g\rangle \otimes 5\rangle$
ψ_{33}	$ g\rangle \otimes 2\rangle$
ψ_{34}	$ g\rangle \otimes 6\rangle$
ψ_{35}	$ g\rangle \otimes 1\rangle$
ψ_{36}	$ g\rangle \otimes 4\rangle$
ψ_{37}	$ g\rangle \otimes 3\rangle$
G_{00}	$ g\rangle \otimes 0\rangle \rightarrow g\rangle \otimes (0\rangle + 7\rangle) + e\rangle \otimes (2\rangle + 5\rangle)$
G_{01}	$ g\rangle \otimes 0\rangle \rightarrow g\rangle \otimes (1\rangle + 6\rangle) + e\rangle \otimes (3\rangle + 4\rangle)$
G_{10}	$ g\rangle \otimes (0\rangle + 7\rangle) \rightarrow g\rangle \otimes 7\rangle + e\rangle \otimes 0\rangle$
G_{11}	$ g\rangle \otimes (2\rangle + 5\rangle) \rightarrow g\rangle \otimes 5\rangle + e\rangle \otimes 2\rangle$
G_{12}	$ g\rangle \otimes (1\rangle + 6\rangle) \rightarrow g\rangle \otimes 6\rangle + e\rangle \otimes 1\rangle$
G_{13}	$ g\rangle \otimes (3\rangle + 4\rangle) \rightarrow g\rangle \otimes 4\rangle + e\rangle \otimes 3\rangle$

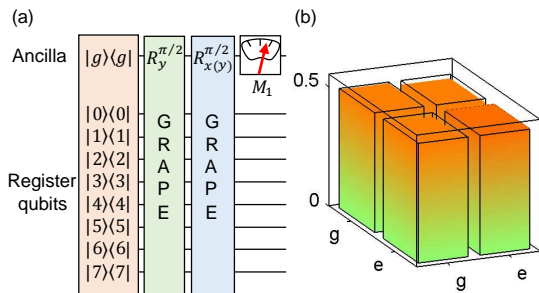


FIG. S2. **Input coherence calibration.** (a) To calibrate the input coherence, we first prepare the maximally-mixed state $\sum_{k=0}^7 |k\rangle\langle k|$ in the storage cavity (the register qubits), then rotate the ancilla qubit to $(|g\rangle + |e\rangle)/\sqrt{2}$ with a pulse numerically optimized with the GRAPE method and independent of photon numbers in the cavity. Finally, we measure the ancilla qubit along X , Y , and Z -axis through pre-rotations $R_{x(y)}^{\pi/2}$ of the ancilla followed by a z -basis measurement. These pre-rotations are also realized by the GRAPE methods and insensitive to the state of the cavity. (b) The experimental density matrix of the ancilla qubit after being prepared in $(|g\rangle + |e\rangle)/\sqrt{2}$ for the initial coherence. The state fidelity is 0.993 and its density matrix contributes 0.894 of the relative entropy of coherence. The solid boxes represent theoretical values.

TABLE II. The measurement-induced phase for each photon number state in the cavity.

photon number state	measurement-induced phase (rad)
$ 1\rangle$	0.31
$ 2\rangle$	0.65
$ 3\rangle$	1.03
$ 4\rangle$	1.43
$ 5\rangle$	1.85
$ 6\rangle$	2.30
$ 7\rangle$	2.78

gives the induced phases by each measurement for different photon number states (TABLE II). To generate the initial register state accurately, we compensate these extra phases induced by the measurement operation in the experiment when optimizing the GRAPE pulses.

- [1] T. Baumgratz, M. Cramer, and M. B. Plenio, “Quantifying coherence,” *Phys. Rev. Lett.* **113**, 140401 (2014).
- [2] A. Streltsov, G. Adesso, and M. B. Plenio, “Colloquium : Quantum coherence as a resource,” *Rev. Mod. Phys.* **89**, 041003 (2017).
- [3] L. Henderson and V. Vedral, “Classical, quantum and total correlations,” *Journal of physics A: mathematical and general* **34**, 6899 (2001).
- [4] H. Ollivier and W. H. Zurek, “Quantum discord: A measure of the quantumness of correlations,” *Phys. Rev. Lett.* **88**, 017901 (2001).
- [5] K. Modi, A. Brodutch, H. Cable, T. Paterek, and V. Vedral, “The classical-quantum boundary for correlations: Discord and related measures,” *Rev. Mod. Phys.* **84**, 1655 (2012).
- [6] G. Adesso, T. R. Bromley, and M. Cianciaruso, “Measures and applications of quantum correlations,” *Journal of Physics A: Mathematical and Theoretical* **49**, 473001 (2016).
- [7] C. C. Rulli and M. S. Sarandy, “Global quantum discord in multipartite systems,” *Phys. Rev. A* **84**, 042109 (2011).
- [8] S. Lloyd and L. Viola, “Engineering quantum dynamics,” *Phys. Rev. A* **65**, 010101 (2001).
- [9] C. Shen, K. Noh, V. V. Albert, S. Krastanov, M. H. Devoret, R. J. Schoelkopf, S. M. Girvin, and L. Jiang, “Quantum channel construction with circuit quantum electrodynamics,” *Phys. Rev. B* **95**, 134501 (2017).
- [10] E. Andersson and D. K. L. Oi, “Binary search trees for generalized measurements,” *Phys. Rev. A* **77**, 052104 (2008).
- [11] N. Khaneja, T. Reiss, C. Kehlet, T. Schulte-Herbrüggen, and S. J. Glaser, “Optimal control of coupled spin dynamics: design of NMR pulse sequences by gradient ascent algorithms,” *J. Magn. Reson.* **172**, 296 (2005).
- [12] P. de Fouquieres, S. Schirmer, S. Glaser, and I. Kuprov, “Second order gradient ascent pulse engineering,” *J. Magn. Reson.* **212**, 412 (2011).

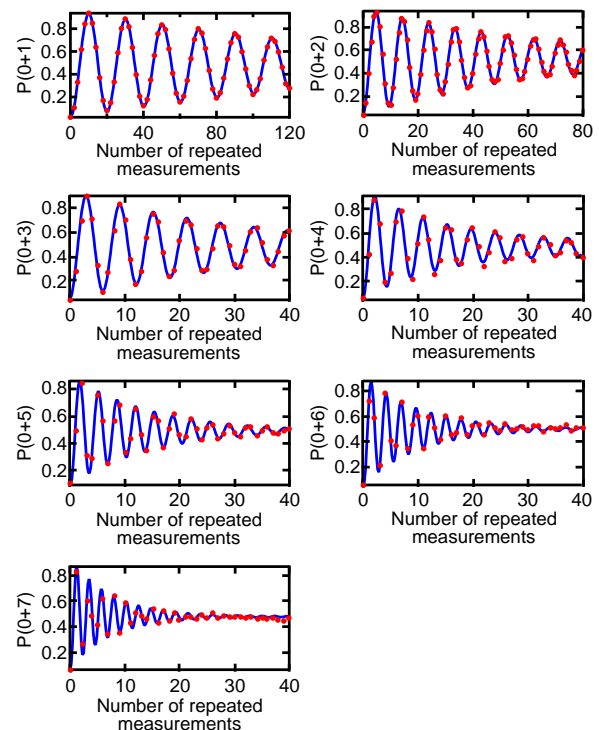


FIG. S3. **Calibration of the measurement-induced phases.** The registers are first prepared in $(|0\rangle + |1\rangle)/\sqrt{2}$, $(|0\rangle + |2\rangle)/\sqrt{2}$, ..., $(|0\rangle + |7\rangle)/\sqrt{2}$ respectively, and then the probabilities $p(0+N)$ of the registers along the corresponding basis of $(|0\rangle + |1\rangle)/\sqrt{2}$, $(|0\rangle + |2\rangle)/\sqrt{2}$, ..., $(|0\rangle + |7\rangle)/\sqrt{2}$ are measured after repeated implementations of measurement operations. Dots are experimental data and solid lines are fit with damped sinusoidal functions.